


Direct observation of the electronic structure of the layered phosphide superconductor $\text{ZrP}_{2-x}\text{Se}_x$ A. Ino *Kurume Institute of Technology, 2228-66 Kamitsu, Kurume, Fukuoka 830-0052, Japan
and Hiroshima Synchrotron Radiation Center, Hiroshima University, Higashi-Hiroshima 739-0046, Japan*

T. Kubo, S. Ishizaka, H. Takita, and W. Mansuer

*Department of Physical Science, Graduate School of Science, Hiroshima University, Higashi-Hiroshima 739-8526, Japan*K. Shimada *Hiroshima Synchrotron Radiation Center, Hiroshima University, Higashi-Hiroshima 739-0046, Japan*S. Ueda *Synchrotron X-ray Station at SPring-8, National Institute for Materials Science (NIMS), Sayo, Hyogo 679-5148, Japan;
Research Center for Advanced Measurement and Characterization, NIMS, Tsukuba 305-0047, Japan;
and Research Center for Functional Materials, NIMS, Tsukuba 305-0044, Japan*H. Kitô , I. Hase, S. Ishida , K. Oka, H. Fujihisa , Y. Gotoh , Y. Yoshida , A. Iyo , H. Ogino , and H. Eisaki*National Institute of Advanced Industrial Science and Technology (AIST), Tsukuba, Ibaraki 305-8568, Japan*

K. Kawashima and Y. Yanagi

IMRA JAPAN Co., Ltd., Kariya, Aichi 448-8650, Japan

(Received 29 May 2021; revised 7 April 2022; accepted 11 April 2022; published 9 May 2022)

A layered phosphide superconductor, $\text{AP}_{2-x}\text{X}_x$ ($A = \text{Zr}$ and Hf ; $X = \text{Se}$ and S), is expected to be a foothold for the quest of new superconductors. Here, we report direct experimental observation of the electronic structure of $\text{ZrP}_{2-x}\text{Se}_x$ ($x = 0.55, 0.60, 0.75, \text{ and } 0.85$), using high-resolution bulk-sensitive hard x-ray photoemission spectroscopy. Core-level spectra of P show two distinct components separated by an energy of 1.2 eV. These reveal that the P atoms at two crystallographic sites have different valence charges, -1 and -3 , playing different chemical roles, and furthermore that the occupation ratio between them varies monotonically with x . We observed valence-band features at -6.5 , -4.0 , and -1.4 eV together with a clear Fermi edge. The consistency with first-principles calculation indicates that the electronic states at Fermi level are mainly ascribed to the Zr $4d$ band. Notably, a hump feature near the Fermi level shows an upward energy shift by 0.49 eV with decreasing x from 0.85 to 0.55. The energy shifts of spectral features substantiate that replacing Se^{2-} with P^{3-} serves as hole doping, shedding light on the tunability of $\text{ZrP}_{2-x}\text{Se}_x$. These findings on the electronic structure establish an essential basis for understanding the superconductivity in the $\text{AP}_{2-x}\text{X}_x$ system.

DOI: [10.1103/PhysRevB.105.195111](https://doi.org/10.1103/PhysRevB.105.195111)**I. INTRODUCTION**

Over recent decades, diversity of superconducting materials has been expanding. The discovery of cuprate superconductors was a breakthrough from alloy to oxide superconductors [1]. The next impact was made by iron-based superconductors [2], which further increased diversity in the base element, anion series, electron filling of d orbitals, and even the phase diagram. In view of the various kinds of the superconductors, it is suggested that the ingredients, which are likely favorable for the superconducting materials, are as follows: (i) two-dimensional layered crystal structure, (ii) tunability of carrier concentration with methods, such as

elemental substitution, and (iii) combination of a transition-metal cation and relatively light anions.

In 2014, a new family of superconductors had been unveiled by Kitô and co-workers [3,4]. The chemical formula is expressed as $\text{AP}_{2-x}\text{X}_x$, where A stands for Zr or Hf, and X stands for a chalcogen, Se, or S. Whereas the superconducting critical temperature T_c was reported to be 6.3 K for $\text{ZrP}_{1.25}\text{Se}_{0.75}$, some implicative features have attracted researchers' interest. First, the crystal structure is the same PbFCl type [3,4] as that of an iron-based superconductor LiFeAs [5–7]. The structure of $\text{ZrP}_{2-x}\text{Se}_x$, for instance, is an alternate stack of a two-dimensional phosphorus plane and a zirconium selenide buckled double layer. Second, optimization for the superconductivity is made by elemental substitution [3,4,8]. Whereas a stoichiometric compound of ZrPSe is rather difficult to synthesize, replacing 25% of Se

*ino@kurume-it.ac.jp

with additional P leads to an increase in T_c , and, in a phase diagram, T_c draws a domelike curve as a function of x in analogy with copper- and iron-based superconductors. Further optimization was achieved in 2018 by nonmagnetic rare-earth substitution for Zr, and, as a result, $T_c = 7.6$ K was recorded for $\text{Zr}_{0.75}\text{Sc}_{0.25}\text{P}_{1.25}\text{Se}_{0.75}$ [9,10]. Third, the combination of Zr and P allows for the interplay of strong electron correlation and a conventional phononic effect. For these reasons, $\text{ZrP}_{2-x}\text{Se}_x$ has been considered as a foothold for the quest of new superconductors.

However, little is known about the electronic structure of the nonstoichiometric $\text{ZrP}_{2-x}\text{Se}_x$ superconductors. Although the first-principles calculation has been reported in Refs. [4,11], the effect of P substitution for Se has been inferred from the electronic structure calculated for $\text{Zr}(\text{As}_{1-x}\text{Se}_x)\text{P}$ within a simple virtual-crystal approximation. From the empirical point of view, even the valence charges of P and Zr atoms remain unclear. The polyvalency of these elements may provide major uncertainties in constructing an effective model for the low-energy electronic states. In particular, in order to clarify the role of the elemental substitution in the superconductivity, we definitely need direct observation of the electronic structure as well as the calculation.

In this paper, we report a systematic photoemission study of the layered zirconium-phosphide-chalcogenide superconductors, $\text{ZrP}_{2-x}\text{Se}_x$ ($x = 0.55, 0.60, 0.75,$ and 0.85). We performed hard x-ray photoemission spectroscopy (HAXPES) [12,13], which is suitable for the first investigation of the electronic structure because of its bulk sensitivity, high throughput, and wide energy scope covering from deep core levels up to the Fermi level, E_F . Whereas core-level spectra shed light on the distinction between the phosphori at two inequivalent sites, valence-band spectra substantiate the fundamental picture of low-energy electronic structure. In light of the findings from continuous spectral evolution with x , we discuss the effect of the P substitution for Se in the nonstoichiometric $\text{ZrP}_{2-x}\text{Se}_x$ superconductor.

II. EXPERIMENT

Well-sintered high-density samples of $\text{ZrP}_{2-x}\text{Se}_x$ ($x = 0.55, 0.60, 0.75,$ and 0.85) were obtained by a high-pressure synthesis technique using a cubic-anvil-type apparatus. The maximum T_c of 6.3 K was observed for $x = 0.75$. Details of the sample preparation and the x dependence of T_c have already been reported in Refs. [3,4].

The HAXPES experiments were performed at the undulator beamline BL15XU of SPring-8 using excitation photons of energy of $h\nu = 5.95$ keV [12]. The electron inelastic mean free path (IMFP) for 6 keV, which is relevant to valence-band and shallow-core photoemission spectra, is typically 90 Å [14,15]. According to the established form of energy dependence, the IMFP for 4 keV, which is relevant to deep-core P 1s spectra, is reduced to 70% of that for 6 keV [14,15]. The spectra were collected with a hemispherical electron analyzer (VG-Scienta R4000 HKE), and the energy resolution was set to ~ 230 and ~ 150 meV for core-level and valence-band spectra, respectively. The experimental geometry of the beamline and the end station was described in Ref. [12]. The

analyzer-lens axis was set in a direction, which is perpendicular to the photon beam and parallel to the electrical field vector of the linearly polarized photons. The incidence and emission angles from the sample normal were typically $\sim 80^\circ$ and $\sim 10^\circ$, respectively. Right before the measurement, the sample surface was scraped off with a diamond file in the preparation chamber and then transferred into the main chamber with the base pressure of $\sim 2 \times 10^{-8}$ Pa. The sample temperature was cooled down and kept at 20 K during the measurement. The energy was calibrated with the Fermi edge of evaporated gold film and is expressed here as that relative to E_F . Cleanness of the samples was confirmed by the absence of the O 1s and C 1s core-level peaks.

First-principles calculation of the electronic structure was performed for stoichiometric material of ZrPSe ($x = 1$). The calculation is based on the full-potential linearized augmented plane wave method and the local-density approximation. These were implemented by computer codes KANSAI-94 and TSPACE [16]. Details of the calculation are described in Ref. [4].

III. RESULTS

A. Core levels

The valence of the phosphorus atom may vary from -3 to $+5$, depending on the circumstances. Thus, we investigate the HAXPES spectra of phosphorus core levels of $\text{ZrP}_{2-x}\text{Se}_x$. Figure 1(a) reveals that two distinct peaks of a deep 1s core level have been observed, even though spin-orbit splitting never occurs for the s orbital. The color gradation from blue to red denotes the decrease in x from 0.85 to 0.55 in Fig. 1. An additional peak is found at 1.3 eV above the main peak at -2143.0 eV, and its intensity increases with substituting P for Se. These findings are reproduced by sharper spectra of the P 2p core level as shown in Fig. 1(b). In principle, the spectral peak of p orbital splits into an intensity ratio of 2:1 by spin-orbit interaction. The main peaks observed at -129.3 and -130.2 eV are assigned to $p_{3/2}$ and $p_{1/2}$ states, respectively. A well-resolved additional peak is observed at 1.2 eV above each of the main peaks, and shows a systematic increase in intensity with substituting P for Se. As x decreases from 0.85 to 0.55, no significant shift was identified for the main peak of P 2p_{3/2}, whereas a small upward shift of about ~ 0.1 eV was detected for the additional peak of P 2p_{3/2}. We also observed the P 2s spectra and found that the relative energy and intensity of an additional component are similar to those of the P 1s and 2p spectra.

In order to quantify the intensity ratio, we performed a fitting analysis of the core-level spectra. As typical results, the extracted peak components for $x = 0.55$ are shown by color filled and hatched areas at the bottom of each panel in Fig. 1. Focusing on the P core-level spectra, the intensity ratio of the additional to main component has been determined for each x as shown in Fig. 2(a). The results from the 1s and 2p_{3/2} peaks are identical to each other within a statistical error, suggesting that this intensity ratio is independent of surface or bulk because the photoelectron kinetic energy and escape depth are different between the shallow-core 2p_{3/2} and deep-core 1s levels.

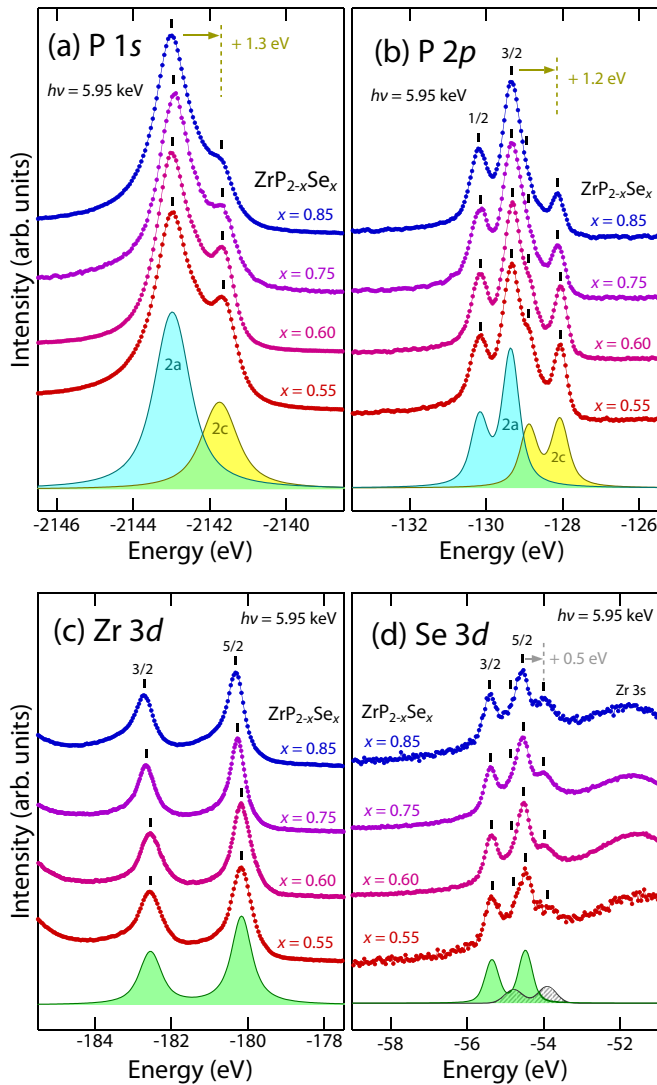


FIG. 1. Core-level spectra of $\text{ZrP}_{2-x}\text{Se}_x$. (a) P $1s$ level. (b) P $2p$ level. (c) Zr $3d$ level. (d) Se $3d$ level. Color filled and hatched areas at each bottom show the peak components extracted by fitting analysis for $x = 0.55$.

Furthermore, Fig. 2(a) clearly shows a linear relationship between the intensity ratio and x , providing evidence that two spectral components arise from two crystallographic sites for P. In fact, previous x-ray diffraction studies have reported that P atoms are located at two sites, which are named $2a$ and $2c$ after the Wyckoff positions [3,4]. The former site is on the two-dimensional P plane, and the latter site is shared with the Se atom as shown in Fig. 2(b). Assuming that the in-plane $2a$ sites are fully occupied by P atoms and that all the rest of P and Se atoms occupy the $2c$ sites as a mixture of $(1-x)\text{P} + x\text{Se}$, we expect that the ratio of P($2c$) to P($2a$) is $1-x$ as drawn with a black dashed line in Fig. 2(a). Notably, the x dependence of the intensity ratios $I_{\text{P}(2c)}/I_{\text{P}(2a)}$ is basically reproduced by this model function $1-x$. A small deviation from $1-x$ is likely due to the defects of the P atom at the in-plane $2a$ sites because such defects have been reported to occur by about 10% for the $2a$ sites of the similar isostructural mixed-anion materials, $\text{ZrAs}_{1.4}\text{Se}_{0.5}$ and $\text{HfAs}_{1.7}\text{Se}_{0.2}$ [17,18]. The linear-fit extrapolation of the experimental data

gives $I_{\text{P}(2c)}/I_{\text{P}(2a)} = 0.14$ at $x = 1$, implying that, even in a stoichiometric sample of ZrPSe , about 12% of P atoms would drop out of the $2a$ site and enter in the $2c$ site.

The energy difference of eV order for the same core orbital suggests that the phosphori at the $2a$ and $2c$ sites are distinguished by valence charge Q_{P} . In practice, the database of core-level energies has served as a simple measure of valence charge [19]. Concerning the energy of the P $2p$ level, a series of first-row transition-metal monophosphide alloys has systematically been studied by photoemission spectroscopy [20,21]. Following the work by Grosvenor *et al.* [20], we adopted an empirical linear relation between the energy of P $2p_{3/2}$ and the valence charge Q_{P} as shown in Fig. 2(c). The data of TiP and ScP [21] were plotted together with the formal P valence of -3 . In this paper, the peaks of P $2p_{3/2}$ were observed at -129.3 and -128.1 eV, which lead to $Q_{\text{P}} = -1$ and -3 for P($2a$) and P($2c$), respectively.

This result can be explained in terms of electronegativity, which is better defined than the valence charge. Considering that the Allred-Rochow electronegativity [22] of P, $\chi(\text{P}) = 2.06$, is sufficiently higher than that of Zr, $\chi(\text{Zr}) = 1.22$, the Zr-P bond has an ionic character in contrast to the covalent in-plane P-P bond, and, thus, the P($2c$) atom surrounded by Zr should capture more negative charge than the in-plane P($2a$) atom. Empirically, it has been established that the core-level energy shift due to interatomic bonding is directly related to the electronegativity difference between two bonded atoms [20]. Given that $\chi(\text{Zr}) = 1.22$ is intermediate between $\chi(\text{Sc}) = 1.20$ and $\chi(\text{Ti}) = 1.32$, the P $2p_{3/2}$ energy of ZrP would also be intermediate between those of ScP and TiP . Hence, the result in Fig. 2(c) suggests that the P($2c$) atom in $\text{ZrP}_{2-x}\text{Se}_x$ has nearly the same valence charge as that in ZrP . Therefore, it is reasonable to assume the formal valence of P($2c$) to be -3 . In light of the formal valences, we can express $\text{ZrP}_{2-x}\text{Se}_x$ as the combination of two-dimensional covalent P^- planes and somewhat ionic $\text{Zr}^{3+}\text{Se}^{2-}$ layers and, furthermore, expect that replacing Se^{2-} with P^{3-} at the $2c$ site serves as hole doping for the low-energy electronic states.

For comparison, core-level spectra representative of the other atoms Zr and Se are shown in Figs. 1(c) and 1(d), respectively. The Zr $3d$ spectra in Fig. 1(c) show only two sharp peaks $d_{5/2}$ and $d_{3/2}$, which were identified as the result of standard spin-orbit splitting because all the spectra are excellently fitted with two Voigt peaks without assuming additional components. The Se $3d$ spectra in Fig. 1(d) show that two main peaks $d_{5/2}$ and $d_{3/2}$ are sharp enough, whereas a small additional component is recognized at 0.5 eV above the main component. In contrast to the P $1s$ and $2p$ spectra, no systematic x dependence of the intensity of the additional component has been identified for the Se $3d$ spectra despite our careful x -dependent experiments. Therefore, it is rather difficult to interpret this additional component in the Se $3d$ spectra in terms of the substitution of P for Se. Instead, we currently consider that the small additional component in the Se $3d$ spectra is ascribed to the emission from the surface Se atoms because we observed that this component is apparently enhanced in our preliminary experiment using vacuum ultraviolet as excitation photons. Note that the Se atoms are most likely to be exposed at surface because of the Coulomb repulsion between two negatively charged Se^{2-}

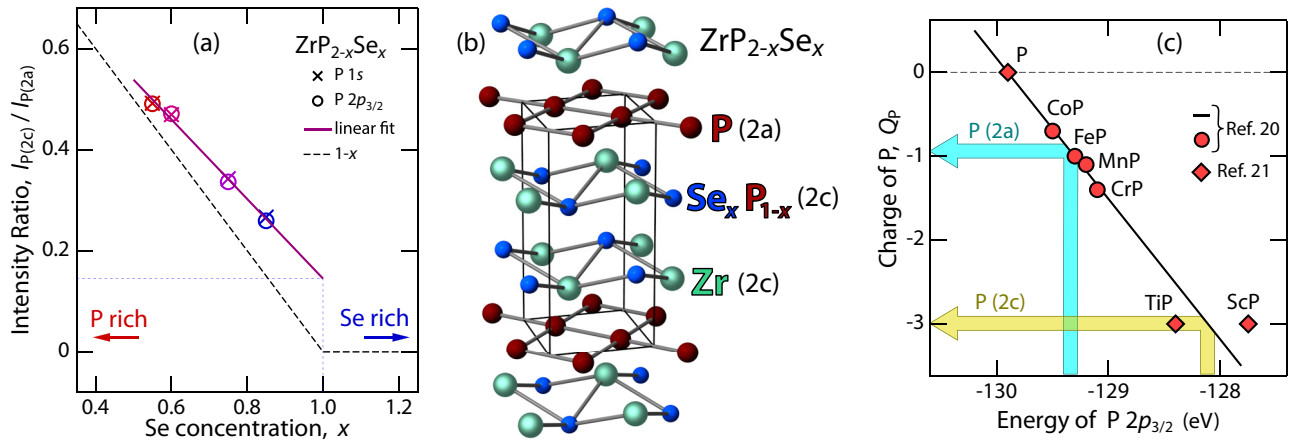


FIG. 2. Findings from the core-level spectra of phosphorus. (a) Intensity ratio of P(2c) to P(2a) peaks, $I_{P(2c)}/I_{P(2a)}$, plotted as a function of x . Crosses (x) and circles (o) denote the experimental data from P 1s and P 2p_{3/2} peaks, respectively. Black dashed and solid lines show a simple model function $1-x$ and the linear fit of experimental data, respectively. (b) Crystal structure of ZrP_{2-x}Se_x from Refs. [3,4]. Two sites for P are named 2a and 2c. (c) Relation between the valence charge of P, Q_P , and the energy of the P 2p_{3/2} core level. Solid line follows the work by Grosvenor *et al.* [20]. Circles and diamonds show the data of first-row transition-metal monophosphide alloys from Refs. [20,21], respectively. Our spectra of P 2p_{3/2} indicate that $Q_P = -1$ and -3 for P(2a) and P(2c), respectively.

layers as seen from Fig. 2(b). It has been reported for ZrSiS, which is isostructural with ZrPSe, that the cleavage plane is between two adjacent chalcogen layers [23]. Regarding the energy shift of the main peaks, we found that the 3d core levels of Zr and Se shift upward by about 0.15 and 0.1 eV, respectively, with decreasing x from 0.85 to 0.55.

B. Valence band

Next, we move on to a valence-band region. The HAXPES spectra in Fig. 3 show the valence-band bottom at -7.7 eV,

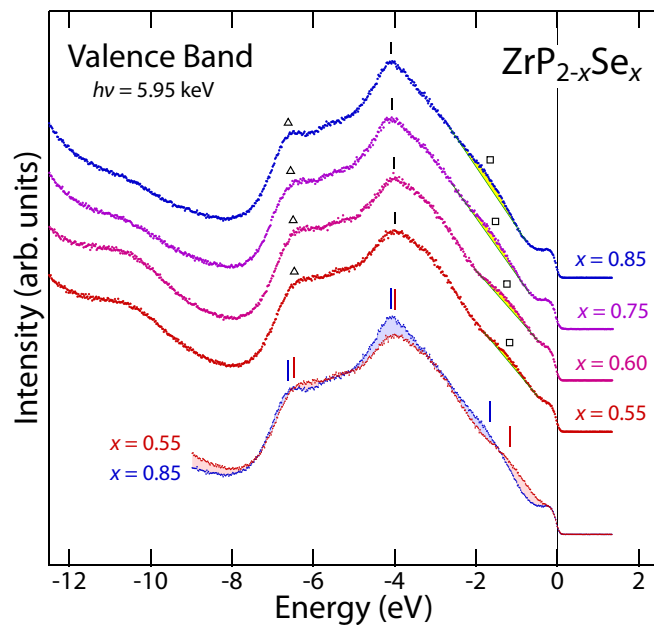


FIG. 3. Valence-band spectra of ZrP_{2-x}Se_x. Typical energies are marked by Δ , $|$, and \square . The spectra of $x = 0.55$ and 0.85 are overlaid at the bottom for comparison between the Se-rich and P-rich ends. Spectral intensity for each x is normalized to the valence-band spectral area.

a cusplike shoulder at -6.5 eV (Δ), an intensity peak at -4.0 eV ($|$), a humplike broad shoulder at -1.4 eV (\square), and a clear Fermi edge, which is consistent with metallic

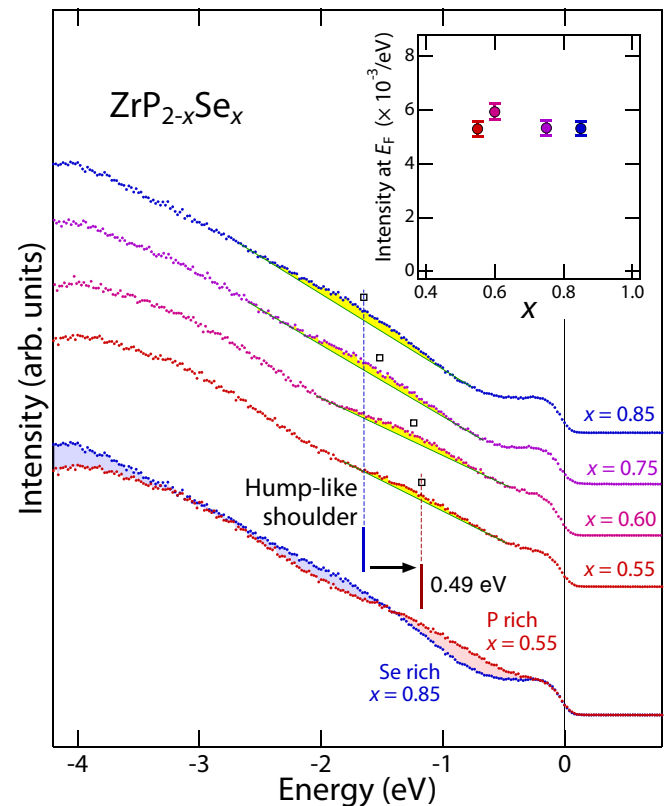


FIG. 4. The same as Fig. 3, but the region including the hump and Fermi edge is enlarged three times in energy. Yellow filled areas denote a spectral hump with respect to a straight slope line. The inset shows the Fermi-edge intensity determined at -0.2 eV. The intensity for each x is normalized so that the valence-band spectral area above -7.7 eV is equal to 1.

transport properties of $\text{ZrP}_{2-x}\text{Se}_x$ [4,24]. The overview of these valence-band features is consistent throughout the range of $0.55 \leq x \leq 0.85$. Considering that the valence electrons originate from the outermost atomic orbitals, the main part of the valence band is ascribed to Se $4p$, P $3p$, and Zr $4d$ bands. Slightly below the valence-band bottom, a broad feature at -10.5 eV increases in intensity with P substitution and, thus, is attributed to the P $3s$ band.

A consistent quality of the sample preparation and the HAXPES measurement have enabled us to identify rather small but appreciable changes with x . Overlaid spectra at the bottom of Fig. 3 demonstrate that the difference between both ends of x is substantial. As x decreases, the peak top at -4.0 eV is rounded and decreases in intensity, indicating a predominance of a character of the Se $4p$ orbital. We found that the peak at -4.0 eV and the cusp at -6.5 eV shift upward by about 0.1 and 0.15 eV, respectively, with decreasing x from 0.85 to 0.55. Strikingly, the humplike shoulder at -1.4 eV shifts more rapidly than the other spectral features. Figure 4 shows an enlarged view of this hump. As x decreases, the yellow-colored hump feature gradually and steadily moves toward E_F , and the amount of energy shift from $x = 0.85$ to 0.55 is as large as 0.49 eV. Another presentation is given by the overlaid spectra at the bottom of Fig. 4. In going from -3 eV toward E_F , the spectral difference switches from negative (blue) to positive (red) at -1.4 eV. This is a typical sign that the hump feature shifts in energy. In addition, whereas a flat region of spectral intensity is seen between -0.6 eV and the Fermi edge for $x = 0.85$, it has been covered by a leading slope for $x = 0.55$, again supporting that the shift of hump is of the order of a half electronvolt. Regarding the spectral intensity at E_F , no obvious x dependence was identified for the present HAXPES experiment as shown in the inset of Fig. 4.

Comparison of experiment and calculation would provide insights into the nature and reality of $\text{ZrP}_{2-x}\text{Se}_x$. Thus, we have simulated the valence-band HAXPES spectrum of $\text{ZrP}_{1.15}\text{Se}_{0.85}$ from the first-principles calculation for ZrPSe by a standard method. First, a rigid-band shift by 0.14 eV is applied to the calculated density of states (DOS) so that the holes doped by replacing 15% of Se^{2-} with P^{3-} are accommodated. The total and partial DOSs at this step are shown in the middle row of Fig. 5. Second, the calculated partial DOS is weighted by the orbital-specific photoemission cross-section given for $h\nu = 5.95$ keV with consideration of the angular distribution [25], and then the summation is taken over all the valence orbitals, i.e., Zr $5s$, Zr $4p$, Zr $4d$, P $3s$, P $3p$, Se $4s$, and Se $4p$. Finally, the calculated spectrum is multiplied by a Fermi-Dirac distribution function and broadened with a convolution of Gaussian and Lorentzian. Specifically, the Gaussian width is set as a constant to represent energy-independent experimental broadening, and the Lorentzian full width at half maximum is given by a form of $0.1|E|$ proportional to energy so that the effect of lifetime broadening is approximated in a simple conventional way [13,26–30]. The simulated spectrum is compared with the experimental one at the top of Fig. 5. The energies and intensities of the valence-band bottom, the cusp, the peak, the hump, and the clear Fermi edge are essentially reproduced by our simulation, although some parts of the experimental spectrum are unexpectedly broader than the simulated one. The broadness of the experimental valence-

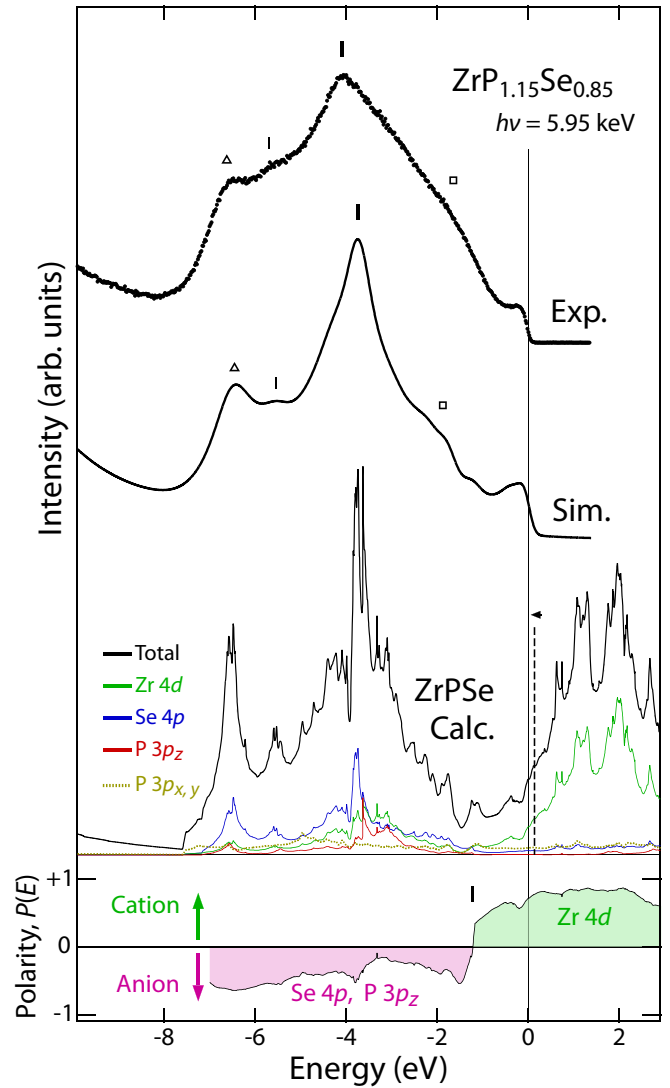


FIG. 5. Top: comparison between the experimental HAXPES spectrum of $\text{ZrP}_{1.15}\text{Se}_{0.85}$ and that simulated from calculation. The secondary background is removed from the experimental spectrum for comparison. Middle: the total DOS and the partial DOSs of Zr $4d$, Se $4p$, P $3p_z$, and P $3p_{x,y}$, obtained from the first-principles calculation for stoichiometric ZrPSe with a rigid band shift by 0.14 eV. Bottom: the energy dependence of the polarity between the cation and the anion states from calculation.

band spectra may arise from the lattice disorder, which is inevitably introduced by the fractional substitution of P for Se. Another possible origin of this discrepancy concerns the approximation in the simulation. Specifically, as indicated by recent HAXPES studies, applying the atomic values of cross sections to the first-principles partial DOS of solid-state materials tends to underestimate the spectral intensity of the s -orbital components in comparison with the results of the experiments and the one-step calculation [13,31]. Focusing on the low-energy region, the simulated spectrum in Fig. 5 implies that the change in the Fermi-edge intensity is hardly observed for the rigid-band shift by ~ 0.5 eV in agreement with the result shown in Fig. 4. The essential consistency between the experiment and the calculation supports their

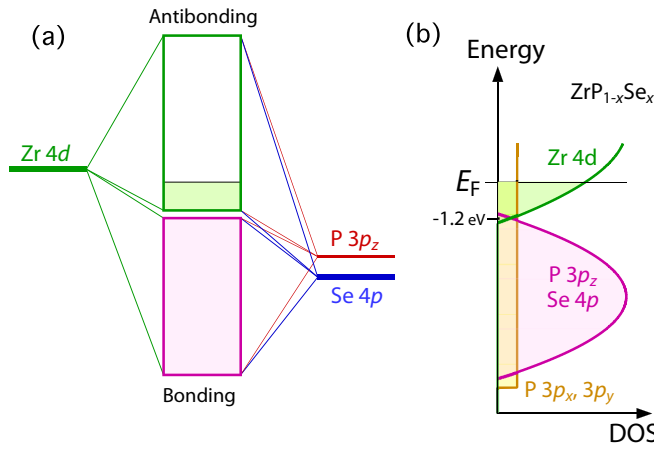


FIG. 6. (a) Schematic energy diagram for ZrPSe. (b) Simplified model of DOS based on the present study of $\text{ZrP}_{2-x}\text{Se}_x$.

validity and allows us to further discuss the orbital character of the valence band.

The energy dependence of the bonding and antibonding characters is evaluated in terms of the cation and anion DOSs. For this purpose, we adopt the Zr 4d states as the cation DOS, $D_c(E) = D_{\text{Zr}4d}(E)$, the Se 4p and P 3p_z states as the anion DOS, $D_a(E) = D_{\text{Se}4p}(E) + D_{\text{P}3p_z}(E)$, and define the cation-anion polarity, $P(E)$ by a form of

$$P(E) = \frac{D_c(E) - D_a(E)}{D_c(E) + D_a(E)}.$$

As shown in the bottom of Fig. 5, the sign of $P(E)$ changes at -1.2 eV. This indicates that the energy region below -1.2 eV is dominated by anion characters (magenta) of Se 4p and P 3p_z as a bonding band and that the energy region above -1.2 eV including E_F is dominated by a cation character (green) of Zr 4d as an antibonding band.

IV. DISCUSSION

Now, let us draw some pictures of the fundamental electronic structure of $\text{ZrP}_{2-x}\text{Se}_x$. Figure 6(a) schematizes the hybridization between the cation and the anion orbitals in the stoichiometric ZrPSe. The bonding band mainly derives from the Se 4p and P 3p_z orbitals, whereas the antibonding band is dominated by a character of the Zr 4d orbital. The P 3p_x and 3p_y orbitals are confined within the two-dimensional P plane and, thus, omitted in Fig. 6(a). In this light, a simplified model of the DOS is deduced from the calculation in Fig. 5. As illustrated in Fig. 6(b), the concentrated high DOS is formed by the bonding and antibonding bands, whereas the underlying widespread low DOS represents a two-dimensional free-electron-like band of the P 3p_x and 3p_y orbitals. The tails of the bonding and antibonding energy bands overlap each other without an energy gap. Their crossover point is predicted at -1.2 eV by the calculation and indeed observed as a flat region of the spectral intensity near the Fermi edge for $x = 0.85$. Therefore, the electronic states at E_F relevant to the superconductivity is predominantly ascribed to the Zr 4d band for $\text{ZrP}_{2-x}\text{Se}_x$. We speculate that relatively high DOS of the Zr 4d band and high-frequency phonons of covalent phosphorous

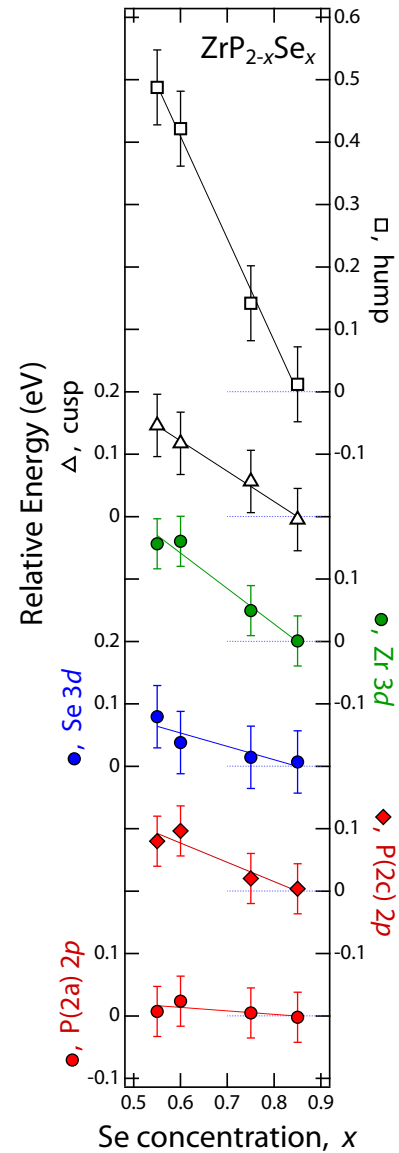


FIG. 7. Energy shifts against x for $\text{ZrP}_{2-x}\text{Se}_x$. Energy is relative to the value of $x = 0.85$. Core-level shifts determined from the peaks of P(2a) 2p_{3/2}, P(2c) 2p_{3/2}, Se 3d_{5/2}, and Zr 3d_{5/2} are denoted by red circles, red diamonds, blue circles, and green circles, respectively. Concerning the valence band, energy shifts of a cusplike shoulder at -6.5 eV and a humplike broad shoulder at -1.4 eV are plotted with black open triangles and squares, respectively.

plane are favorable for the superconductivity. As expected from the basic formulas of the phonon-mediated superconductivity [32], the highly peaked DOS at E_F plays a definitive role in the A15-type superconductors, such as Nb₃Sn [33,34], and the high-frequency phonons are responsible for high- T_c superconductivity in hydrogen sulfides [35].

In order to put the substitution effects into perspective, we plotted together various energy shifts against x in Fig. 7. It is worth noting that all the energy shifts are in the same direction except for the core level of in-plane P(2a). This result makes a contrast with the usual case of elemental substitution where the core-level shifts are in the opposite directions between the anions and the cations [36,37]. As discussed in previous

studies, two major origins of the core-level shift ΔE in a solid is a change in the atomic valence charge ΔQ and a chemical-potential shift $\Delta\mu$ so that we have an approximate formula of $\Delta E \simeq K \Delta Q + \Delta\mu$, where K is a linear coefficient [36,37]. Upon elemental substitution, intersite charge transfer leads to the core-level shifts in the opposite directions between two atomic sites. Therefore, the component common to all the core-level shifts is ascribed to $\Delta\mu$ and, thus, supports that the downward chemical-potential shift is indeed caused by substitution of P^{3-} for Se^{2-} . Quantitatively, the shift rate of the chemical potential is deduced to be $\Delta\mu/\Delta x \simeq 0.3$ eV from the average among the experimental core-level shifts of P(2a) 2p, P(2c) 2p, Se 3d, and Zr 3d, whereas it is expected to be $\Delta\mu/\Delta x = 1.3$ eV from the DOS obtained by the first-principles calculation, suggesting that doping efficiency is lower than expected from the rigid-band model. Compared with the averaged shift, the shift of the Zr 3d level is rapid, and that of P(2a) 2p level is indiscernible. These divergent core-level shifts are attributed to the change in the atomic valence ΔQ , implying that a small amount of electrons is transferred from the in-plane P(2a) to Zr sites as x decreases [36].

On the other hand, the shift of the valence-band hump stands out among the other shifts, as shown in Fig. 7. Even within the valence band, the difference between the hump and the cusp energies indicates that the valence-band width increases as x decreases. It follows that the substitution effect on the valence band deviates from the rigid-band model to some extent. When considering the impact on the superconductivity, the shift of low-energy electronic structure is of primary importance. Hence, the energy shift, $\Delta E/\Delta x \simeq -1.6$ eV, determined from the valence-band hump is most relevant to the electronic states responsible for the superconductivity. This energy shift is large enough to play an essential role in the

mechanism for the x -dependent optimization for the superconductivity in $ZrP_{2-x}Se_x$.

V. CONCLUSION

In conclusion, we have determined the fundamental electronic structure of the layered zirconium-phosphide-chalcogenide superconductors $ZrP_{2-x}Se_x$ from the HAXPES experiments. The fitting analysis of the core-level spectra has revealed that the valence charges of P(2a) and P(2c) are -1 and -3 , respectively, and determined the x dependence of the phosphorus occupation ratio between the 2a and the 2c sites. Key features in the valence-band spectra are consistent with the first-principles calculation, indicating that the electronic states at E_F is mainly ascribed to the Zr 4d band. It is deduced from the energy shifts of the spectral features that the downward chemical-potential shift is realized by substitution of P^{3-} for Se^{2-} at the 2c site, shedding light on the tunability of $ZrP_{2-x}Se_x$. In particular, the rapid energy shift $\Delta E/\Delta x \simeq -1.6$ eV of the low-energy electronic structure is most likely relevant to the substitution effect on the superconductivity. These findings on the electronic structure of $ZrP_{2-x}Se_x$ serve as the first and substantial step for the understanding of a large family of $AP_{2-x}X_x$ superconductors.

ACKNOWLEDGMENTS

We are grateful to A. Kimura for an enlightening discussion. The HAXPES experiments were performed under the approval of the NIMS Synchrotron X-ray Station (Proposals No. 2015A4801, No. 2015B4800, No. 2016A4800, and No. 2017B4801). This work was supported by JSPS KAKENHI Grant No. 20K03842.

-
- [1] J. G. Bednorz and K. A. Müller, *Z. Phys. B* **64**, 189 (1986).
- [2] Y. Kamihara, T. Watanabe, M. Hirano, and H. Hosono, *J. Am. Chem. Soc.* **130**, 3296 (2008).
- [3] H. Kitô, Y. Yanagi, S. Ishida, K. Oka, Y. Gotoh, H. Fujihisa, Y. Yoshida, A. Iyo, and H. Eisaki, *J. Phys. Soc. Jpn.* **83**, 074713 (2014).
- [4] S. Ishida, H. Fujihisa, I. Hase, Y. Yanagi, K. Kawashima, K. Oka, Y. Gotoh, Y. Yoshida, A. Iyo, H. Eisaki, and H. Kitô, *Supercond. Sci. Technol.* **29**, 055004 (2016).
- [5] X. C. Wang, Q. Q. Liu, Y. X. Lv, W. B. Gao, L. X. Yang, R. C. Yu, F. Y. Li, and C. Q. Jin, *Solid State Commun.* **148**, 538 (2008).
- [6] M. J. Pitcher, D. R. Parker, P. Adamson, S. J. C. Herkelrath, A. T. Boothroyd, R. M. Ibberson, M. Brunelli, and S. J. Clarke, *Chem. Commun.*, 5918 (2008).
- [7] J. H. Tapp, Z. Tang, B. Lv, K. Sasmal, B. Lorenz, P. C. W. Chu, and A. M. Guloy, *Phys. Rev. B* **78**, 060505(R) (2008).
- [8] K. W. Chen, G. Chappell, S. Zhang, W. Lan, T. Besara, K. Huang, D. Graf, L. Balicas, A. P. Reyes, and R. E. Baumbach, *Phys. Rev. B* **102**, 144522 (2020).
- [9] K. Iwakiri, T. Nishio, K. Kawashima, S. Ishida, K. Oka, H. Fujihisa, Y. Gotoh, A. Iyo, H. Ogino, H. Eisaki, Y. Yoshida, and H. Kitô, *J. Phys.: Conf. Ser.* **1054**, 012002 (2018).
- [10] K. Iwakiri, T. Nishio, K. Kawashima, S. Ishida, K. Oka, H. Fujihisa, Y. Gotoh, I. Hase, A. Iyo, H. Ogino, H. Eisaki, Y. Yoshida, and H. Kitô, *J. Phys.: Conf. Ser.* **1293**, 012003 (2019).
- [11] I. Hase, T. Yanagisawa, H. Kito, K. Iwakiri, T. Nishio, H. Fujihisa, Y. Gotoh, H. Eisaki, and K. Kawashima, *J. Phys.: Conf. Ser.* **1590**, 012008 (2020).
- [12] S. Ueda, *J. Electron Spectrosc. Relat. Phenom.* **190**, 235 (2013).
- [13] S. Ueda and I. Hamada, *J. Phys. Soc. Jpn.* **86**, 124706 (2017); **90**, 034706 (2021); **91**, 024801 (2022).
- [14] S. Tanuma, C. J. Powell, and D. R. Penn, *Surf. Interface Anal.* **21**, 165 (1994).
- [15] H. Shinotsuka, S. Tanuma, C. J. Powell, and D. R. Penn, *Surf. Interface Anal.* **47**, 871 (2015).
- [16] A. Yanase, *Fortran Program For Space Group (TSPACE)* (Shokabo, Tokyo, 1995) [in Japanese].
- [17] M. Schmidt, T. Cichorek, R. Niewa, A. Schlechte, Y. Prots, F. Steglich, and R. Kniep, *J. Phys.: Condens. Matter* **17**, 5481 (2005).
- [18] A. Czulucki, G. Auffermann, M. Bednarski, Ł. Bochenek, M. Böhme, T. Cichorek, R. Niewa, N. Oeschler, M.

- Schmidt, F. Steglich, and R. Kniep, *ChemPhysChem* **11**, 2639 (2010).
- [19] A. V. Naumkin, A. Kraut-Vass, S. W. Gaarenstroom, and C. J. Powell, NIST X-Ray Photoelectron Spectroscopy Database, NIST Standard Reference Database Number 20 (National Institute of Standards and Technology, Gaithersburg, MD, 2000), doi: <http://dx.doi.org/10.18434/T4T88K>.
- [20] A. P. Grosvenor, S. D. Wik, R. G. Cavell, and A. Mar, *Inorg. Chem.* **44**, 8988 (2005).
- [21] C. E. Myers, H. F. Franzen, and J. W. Anderegg, *Inorg. Chem.* **24**, 1822 (1985).
- [22] A. L. Allred and E. G. Rochow, *J. Inorg. Nucl. Chem.* **5**, 264 (1958).
- [23] L. M. Schoop, M. N. Ali, C. Straßer, A. Topp, A. Varykhalov, D. Marchenko, V. Duppel, S. S. Parkin, B. V. Lotsch, and C. R. Ast, *Nat. Commun.* **7**, 11696 (2016).
- [24] H. Kitô, K. Iwakiri, T. Nishio, K. Kawashima, S. Ishida, K. Oka, H. Fujihisa, Y. Gotoh, A. Iyo, H. Ogino, H. Eisaki, and Y. Yoshida, *J. Phys.: Conf. Ser.* **1054**, 012003 (2018).
- [25] M. Trzhaskovskaya, V. Nefedov, and V. Yarzhemsky, *At. Data Nucl. Data Tables* **77**, 97 (2001).
- [26] A. Fujimori and F. Minami, *Phys. Rev. B* **30**, 957 (1984).
- [27] K. Kobayashi, T. Mizokawa, K. Mamiya, A. Sekiyama, A. Fujimori, H. Takagi, H. Eisaki, S. Uchida, R. J. Cava, J. J. Krajewski, and W. F. Peck, *Phys. Rev. B* **54**, 507 (1996).
- [28] A. Toropova, G. Kotliar, S. Y. Savrasov, and V. S. Oudovenko, *Phys. Rev. B* **71**, 172403 (2005).
- [29] A. X. Gray, D. W. Cooke, P. Krüger, C. Bordel, A. M. Kaiser, S. Moyerman, E. E. Fullerton, S. Ueda, Y. Yamashita, A. Gloskovskii, C. M. Schneider, W. Drube, K. Kobayashi, F. Hellman, and C. S. Fadley, *Phys. Rev. Lett.* **108**, 257208 (2012).
- [30] S. Ueda, M. Mizuguchi, Y. Miura, J. G. Kang, M. Shirai, and K. Takanashi, *Appl. Phys. Lett.* **109**, 042404 (2016).
- [31] D. Takegami, L. Nicolaï, T. C. Koethe, D. Kasinathan, C. Y. Kuo, Y. F. Liao, K. D. Tsuei, G. Panaccione, F. Offi, G. Monaco, N. B. Brookes, J. Minár, and L. H. Tjeng, *Phys. Rev. B* **99**, 165101 (2019).
- [32] J. Bardeen, L. N. Cooper, and J. R. Schrieffer, *Phys. Rev.* **108**, 1175 (1957).
- [33] G. Stewart, *Physica C* **514**, 28 (2015).
- [34] N. S. Sitaraman, M. M. Kelley, R. D. Porter, M. U. Liepe, T. A. Arias, J. Carlson, A. R. Pack, M. K. Transtrum, and R. Sundararaman, *Phys. Rev. B* **103**, 115106 (2021).
- [35] Y. Ge, F. Zhang, and Y. Yao, *Phys. Rev. B* **93**, 224513 (2016).
- [36] A. Ino, T. Mizokawa, A. Fujimori, K. Tamasaku, H. Eisaki, S. Uchida, T. Kimura, T. Sasagawa, and K. Kishio, *Phys. Rev. Lett.* **79**, 2101 (1997).
- [37] N. Harima, A. Fujimori, T. Sugaya, and I. Terasaki, *Phys. Rev. B* **67**, 172501 (2003).